Subensemble decomposition and Markov process analysis of Burgers turbulence

Zhi-Xiong Zhang* and Zhen-Su She
State Key Laboratory of Turbulence and Complex Systems and College of Engineering, Peking University, Beijing 100871, People's Republic of China
(Received 27 May 2011; published 25 August 2011)

A numerical and statistical study is performed to describe the positive and negative local subgrid energy fluxes in the one-dimensional random-force-driven Burgers turbulence (Burgulence). We use a subensemble method to decompose the field into shock wave and rarefaction wave subensembles by group velocity difference. We observe that the shock wave subensemble shows a strong intermittency which dominates the whole Burgulence field, while the rarefaction wave subensemble satisfies the Kolmogorov 1941 (K41) scaling law. We calculate the two subensemble probabilities and find that in the inertial range they maintain scale invariance, which is the important feature of turbulence self-similarity. We reveal that the interconversion of shock and rarefaction waves during the equation's evolution displays in accordance with a Markov process, which has a stationary transition probability matrix with the elements satisfying universal functions and, when the time interval is much greater than the corresponding characteristic value, exhibits the scale-invariant property.

DOI: 10.1103/PhysRevE.84.026326 PACS number(s): 47.27.Gs, 02.50.Ga, 47.27.eb

I. INTRODUCTION

One of the most important features of turbulence is the energy flux or the energy cascade, which has two transfer directions: from large to small scales—(positive) energy flux—derived by Kolmogorov for three-dimensional (3D) turbulence [1], and from small to large scales—negative or inverse energy flux—proposed by Kraichnan for two-dimensional turbulence [2]. These two physical processes exist in most turbulence fields at the same time from a local point of view, as suggested by Kraichnan [3]. Typically, in Burgers turbulence (abbreviated as "Burgulence" by Frisch and Bec [4]), a simplified approximation of the Navier-Stokes equation, the positive and negative local energy fluxes correspond to shock waves and rarefaction waves, respectively. Now, the forced Burgulence has been at the center of studies that allowed unifying different branches of physics and mathematics [5]. Revealing the property of the local energy fluxes is one of the most fundamental problems in turbulence.

In 1939, the Dutch scientist J. M. Burgers introduced a one-dimensional (1D) model for pressureless gas dynamics [6], famously known as the Burgers equation,

$$\frac{\partial u}{\partial t}+\frac{1}{2}\frac{\partial u^2}{\partial x}=\nu\frac{\partial^2 u}{\partial x^2}, \tag{1}$$

which is widely studied in statistical physics, cosmology, and hydrodynamic turbulence today. In the 1950s, Hopf [7] and Cole [8] demonstrated mathematically that the Burgers equation can be integrated explicitly. Later, Meecham and Siegel [9] and Hosokawa and Yamamoto [10] numerically investigated this model with random initial values using the Wiener-Hermite expansion and Hopf theory, respectively. However, its dynamic behavior is fundamentally different from the Navier-Stokes dynamics because of the absence of the pressure term and the local interactions only in x space. To model the pressure, Jeng [11] imposed a random force $f(x,t)$ on the right-hand side of Eq. (1) and found that the numerical velocity field satisfied quasi-Gaussian distribution and the energy spectrum $E(k)\propto k^{-2}$.

Soon after, many important efforts were devoted to the study of the solutions of Burgulence arising from random initial conditions or a random forcing. For the solution of the inviscid Burgers equation with random initial data, Avellaneda and Weinan [12], whose work inspires us to consider Markov process in this paper, rigorously proved some statistical properties for velocities, shock strengths, and rarefaction intervals. For the random forcing, based on renormalization group methods, Forster, Nelson, and Stephen [13] proposed a widely spread, white-in-time random, and zero mean formula in spectral space,

$$\langle\hat{f}(k,t)\hat{f}(k',t')\rangle=2(2\pi)^2Dk^{-1}\delta(k+k')\delta(t-t'), \tag{2}$$

where the circumflex denotes the Fourier representation.

In 1995, Chekhlov and Yakhot [14] numerically studied the random-force-driven Burgers equation again, where the viscous term was replaced by a hyperdissipation form $\nu(-1)^{p+1}\partial^{2p}u/\partial x^{2p}$, and a special group of random forcing parameters was employed. They obtained the remarkable result that the dynamics of the forced equation became more similar to that of Kolmogorov turbulence with a long inertial range, where the energy flux was a constant as the viscosity goes to zero and the energy spectrum satisfied Kolmogorov's $k^{-5/3}$ law [15], but the scaling law was different from Kolmogorov 1941 (K41) prediction $p/3$ [16] and indicated that the higher order correlation functions were still dominated by shocks. Recently, abundant numerical, statistical, and theoretical investigations on forced Burgulence, including the field theory results deduced by Polyakov [17], were reported [17–27], in which many features such as asymmetry probability distribution, anomalous scaling law, and strong intermittence are discussed deeply.

Here, we focus on the statistical scaling behavior and Markov process evolution of Burgulence's shock and rarefaction waves, which correspond to the positive and negative sub-grid-scale energy fluxes, respectively. Section II sketches the Burgulence fields generated using Chekhlov and Yakhot's

*pekingzzx@pku.edu.cn

method [14]. In Sec. III, a subensemble decomposition is used to distinguish the shock wave from the rarefaction wave at different scales. Two different scaling laws are shown, which evinces that the shock wave ensemble has a strong intermittency which dominates the Burgulence intermittency, while the scaling behavior of the rarefaction wave ensemble satisfies K41 theory. In Sec. IV, after certifying the scale invariance of subensemble probabilities, we reveal the interconversion of shock and rarefaction waves during the equation's evolution displays in accordance with a Markov process, which has a stationary transition probability matrix with the elements satisfying universal functions and, when the time interval is much greater than the corresponding characteristic value, exhibits the scale-invariant property. At last, the effects of the random forcing parameter y are represented in Sec. V.

II. DIRECT NUMERICAL SIMULATION FOR BURGULENCE

Using the Fourier-Galerkin pseudospectral method described in Ref. [14], the direct numerical simulation (DNS) for constructing the Burgulence field is sketched as follows. As the governing equation of the velocity signal $u(x,t)$, the random-force-driven Burgers equation is written as

$$\frac{\partial u}{\partial t}+\frac{1}{2}\frac{\partial u^2}{\partial x}=\nu(-1)^{p+1}\frac{\partial^{2p}u}{\partial x^{2p}}+f, \tag{3}$$

where $p=6$ and $\nu=9.0\times10^{-40}$, which are set mainly to obtain a long inertial range. To apply the Fourier-Galerkin pseudospectral method, periodic boundary conditions $\partial^n u(0,t)/\partial x^n=\partial^n u(2\pi,t)/\partial x^n$, $n=0,1,\ldots$, are imposed on the computational domain $x\in[0,2\pi]$.

Then, the random force satisfying Eq. (2) in Fourier space is given as

$$\hat{f}(k,t)=\begin{cases}\dfrac{A_f|k|^{-y/2}\sigma_k}{\sqrt{\Delta t}} & k<k_c,\\ 0 & k\geqslant k_c,\end{cases} \tag{4}$$

where σ_k is the Gaussian random function with $\overline{|\sigma_k|^2}=1$, and other parameters are chosen to be $A_f=\sqrt{2}\times10^{-3}$ and

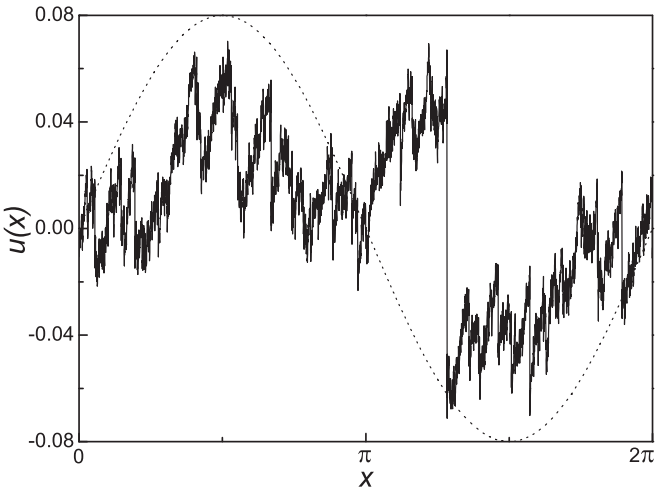

FIG. 1. Velocity signal of the Burgers equation at $t=300$ (solid line) and $t=0$ (dotted line, the initial field).

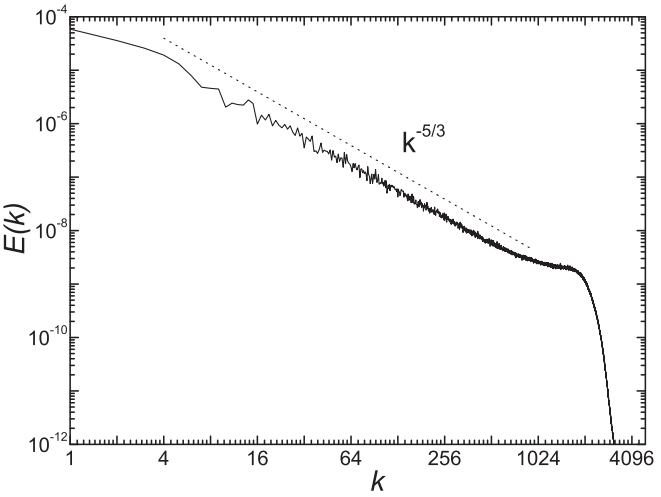

FIG. 2. Energy spectrum averaged in $t\in[100,300]$ (solid line). A dotted line with slope $-5/3$ is also plotted.

$y=1$. The force cutoff k_c is chosen well inside the dissipation range of the energy spectrum, with $k_c=3895$. The time step is set as $\Delta t=5.0\times10^{-5}$.

When implementing the algorithm, the initial field is given by a sine function, $u(x,0)=0.08\sin(x)$. The temporal discretization includes two second-order schemes: the Runge-Kutta scheme for restarting and the stiffly stable Adams-type scheme with the explicit formulation

$$\hat{u}(k,t+\Delta t)=\hat{u}(k,t)+\tfrac{3}{2}\Delta t\hat{g}(k,t)-\tfrac{1}{2}\Delta t\hat{g}(k,t-\Delta t), \tag{5}$$

where $\hat{g}(k,t)=\hat{f}(k,t)-ik[\widehat{u^2}](k,t)/2-\nu k^{2p}\hat{u}(k,t)$.

During the computation, the spatial discretization is based on the pseudospectral method with the nonlinear $[\widehat{u^2}]$ computation in the conservative form and dealiasing procedure based on the 2/3 rule. The spectral resolution employed here is $N=12288$ including the dealiased modes, and the random force generated at different computing time is nonrepeating.

As results, the velocity field at $t=300$ and the average energy spectrum with $t\in[100,300]$ are shown in Figs. 1 and 2, respectively. In the plots, the typical fractal-like and sawtooth structures in the velocity field and the Kolmogorov $k^{-5/3}$ spectrum with a long inertial range are reproduced, which conform well to the results in Ref. [14]. Here, we want to point out that the statistical features of shock and rarefaction waves depend on the random forcing much more than the initial data.

III. SUBENSEMBLE DECOMPOSITION AND CORRESPONDING SCALING LAW

In the traditional generalized opinion, the shock and rarefaction waves in 1D Burgulence can be defined though the speed difference $\delta u(x,l)=u(x+l/2)-u(x-l/2)$, where $x+l/2$ and $x-l/2$ are the starting and ending locations of the corresponding structure. If $\delta u(x,l)>0$, the structure is regarded as a rarefaction wave. On the contrary, if $\delta u(x,l)<0$, the structure is a shock wave. From Burgers' results [28] on the distribution of the separations between rarefaction intervals and the Markovian nature of the equation solution, the set of shock locations, which have no thickness ($l\to0$), is expected

to be countable and discrete. In his case, the structure of shocks depends crucially on the similarity properties of the random initial data. However, in the random-force-driven Burgulence, under the unceasing action of random forcing, the effect on the initial data of the statistical features of shock and rarefaction waves becomes smaller and smaller. From Fig. 1 we can see that the Burgulence field has typical fractal characteristics, since there are shocks in any arbitrary scale rarefaction wave.

Now, we introduce the concept of group velocity difference (GVD), denoted as $h(x,l)$, to identify "new" shock and rarefaction waves from a filtered field point of view. In mathematics, the GVD $h(x,l)$ can be written as the difference of local integrations,

$$h(x,l) = \frac{2}{l}\int_0^{l/2} u(x+l')dl' - \frac{2}{l}\int_{-l/2}^{0} u(x+l')dl'. \quad (6)$$

Moreover, $h(x,l)$ has an equivalence definition as

$$h(x,l) = \frac{1}{l}\int_0^{l} \delta u(x,l')dl' = \delta\widetilde{u}(x,l/2), \quad (7)$$

where the tilde denotes a box filtering. Through the sign of $h(x,l)$, the fluctuation structures in the whole field can be divided into two subensembles, namely,

$$J \in \begin{cases} \text{A} & h(x,l) \geqslant 0, \\ \text{B} & h(x,l) < 0. \end{cases} \quad (8)$$

Here, J marks the structure style; A and B denote the rarefaction wave and shock wave subensembles, respectively. Figure 3 is a sketch of this definition: if its right half group or average velocity is larger or less than the left one, the structure in $[x-l/2, x+l/2]$ with l denoted as the interval size or structure scale is regarded as an element of subensemble A or B.

Without doubt, this decomposition is in accord with the common comprehension about the positive and negative local energy fluxes or the energy cascade. Following Eyink's definition [29], we represent the local energy flux in Burgulence as $\Pi(x,l/2) = -(\widetilde{u^2} - \tilde{u}^2)\partial\tilde{u}(x,l/2)/\partial x$. Approximatively, there is $\Pi(x,l/2) \approx -2(\widetilde{u^2} - \tilde{u}^2)h(x,l)/l$, which means that when $h(x,l) < 0$, $\Pi(x,l/2) > 0$, the energy cascade is forward, from large to small scales; when $h(x,l) \geqslant 0$, $\Pi(x,l/2) \leqslant 0$, the energy cascade is reversed, from small to large scales.

Then, based on above subensemble decomposition, we can investigate the scaling behaviors in each different subensemble, respectively. Following the traditional method, we define the statistical moment function of $h(x,l)$ as

$$Z_p(l) = \langle |h(x,l)|^p \rangle, \quad (9)$$

where $\langle\cdot\rangle$ stands for the ensemble average. From 20 000 statistical stable velocity fields obtained in the previous section with equal time interval and $t \in [100,300]$ (without special explanation, all statistics in this paper are measured from the same 20 000 velocity fields), $Z_p(l)$ for subensembles A and B are measured and plotted in Figs. 4 and 5 with $l/\delta = 2,4,\ldots,1024$ and $p = 1,2,\ldots,8$ [where δ is the physical resolution equal to $2\pi/(2N/3)$ in DNS]. The plots reveal that both subensembles satisfy good absolute scaling law in an inertial range,

$$Z_p(l) \propto l^{\zeta_p}. \quad (10)$$

From Figs. 4 and 5, we can see both subensemble A and subensemble B have the same inertial range: the slope of the line in the log-log plot of Fig. 4 is growing gradually with order number p increasing from 1 to 8, but the slopes of lines in Fig. 5 no longer change after a certain order number $p \approx 3$. Furthermore, we plot out these scaling exponents for subensemble A, subensemble B and the whole field without decomposition in Fig. 6. It is distinctly clear that the scaling behaviors in subensembles A and B are very different from each other.

For subensemble A, the scaling behavior is very approximative to the K41 theorem [16] with

$$\zeta_{p,A}(l) = p/3, \quad (11)$$

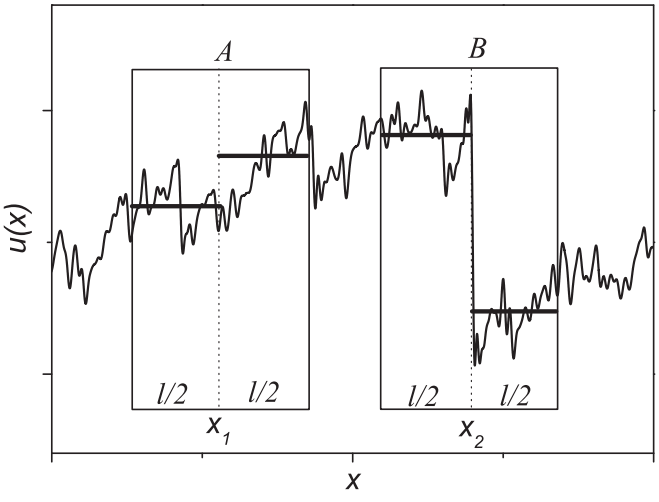

FIG. 3. A sketch for the definition of subensembles A (rarefaction wave) and B (shock wave) using an enlarged segment in Fig. 1 (solid line). The heavy horizontal lines in small boxes state the local group or average velocities.

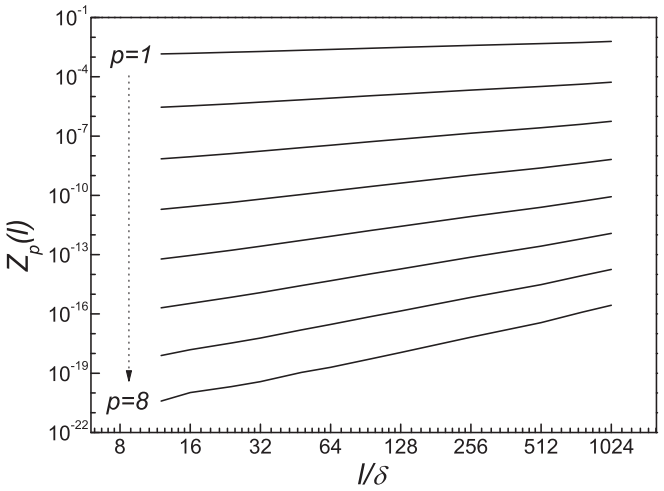

FIG. 4. Structure function for subensemble A (solid line) at different scales $l/\delta = 12,16,\ldots,1024$.

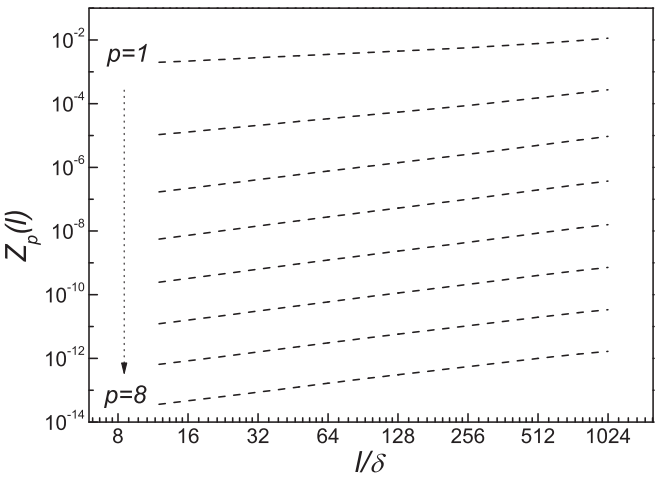

FIG. 5. Structure function for subensemble B (dotted line) at different scales $l/\delta = 12,16,\ldots,1024$.

which means subensemble A has a conspicuous Gaussian property with little intermittence. For subensemble B, an anomalous scaling law is observed:

$$\zeta_{p,B}(l) = p/3, \quad p < 3; \quad \zeta_{p,B}(l) \approx 0.92, \quad p > 3. \tag{12}$$

Evidently, it is more like the typical anomalous scaling law in the Burgers equation and different from either K41 theory [16] or the SL94 model [30]. The scaling exponents in the whole field with $\zeta_p(l) \sim 0.95$ when $p > 3$ are close to those in subensemble B, since the statistical moment function $Z_p(l)$ of subensemble B is much larger than that of subensemble A at the same order number p, which can be confirmed through comparing Fig. 4 with Fig. 5. So it is surprisingly explicit that subensemble B—shocks—dominate the intermittency of Burgulence.

As background, the typical anomalous scaling in the Burgers equation was obtained in Ref. [14], where the scaling exponents ζ_p of the ordinary velocity structure functions, defined by $S_p(l) = \langle |v(x+l) - v(x)|^p \rangle \propto l^{\zeta_p}$, were found to be almost independent of p ($\zeta_p = 0.91$ at $p = 4,6,8$). It is also noted that Mitra *et al.* [27] argued that, in the stochastically forced Burgers equation, they found an artifact in which logarithmic corrections can appear disguised as anomalous scaling and concluded that bifractal scaling is likely. In fact, the probability distribution function (PDF) of $h(x,l)$ in A and B have different properties and the PDF of $h(x,l)$ in B also have algebraic tails, similar to the results discussed in Refs. [19,22,26].

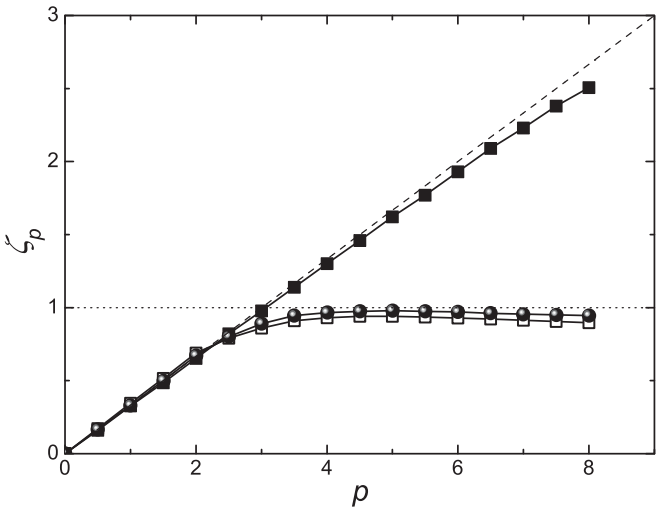

FIG. 6. Exponents of structure function for subensemble A (solid squares), subensemble B (open squares), and the whole field (solid circles). The dashed and dotted lines correspond to $\zeta_p = p/3$ and $\zeta_p = 1$, respectively.

The above results signal that, through subensemble decomposition, the difference between shock and rarefaction waves within the same dynamical system—Burgulence—can be clearly revealed from corresponding statistical scaling behaviors. In other words, the two kinds of self-organization processes, the positive and negative local energy fluxes, in Burgulence have extremely different states: one has little intermittence, but the other has strong intermittence; one has Gaussian properties, but the other does not. When they are mixed together, one of them may be obscured in the whole system behavior, which is witnessed by the scaling law shown in Fig. 6.

IV. MARKOV PROCESS EVOLUTION BETWEEN TWO SUBENSEMBLES

Based on the subensemble definition above, we employ the Markov process analysis to describe the transition between the positive and negative local energy fluxes. For a velocity field $u(x,t)$ at fixed t with $x \in [0,2\pi]$, it is easy to count the probability of subensembles at structure scale l:

$$P_A(l,t) = P(h(x,l,t) \geqslant 0 | x \in [0,2\pi]), \tag{13}$$

$$P_B(l,t) = P(h(x,l,t) < 0 | x \in [0,2\pi]). \tag{14}$$

Obviously, $P_A(l,t) + P_B(l,t) = 1$, and if subensembles A and B have the same probability, we have $P_A(l,t) = P_B(l,t) = 0.5$. But the truth of the matter is quite different.

In fact, $P_A(l,t)$ is distinctly greater than $P_B(l,t)$ at the statistical equilibrium state of Burgulence, in which the probabilities rarely change after time $t = 100$, though they are fluctuating with time going forward. Figure 7 shows the time-averaged probabilities of subensembles A and B at different scales with error bars marked by the standard deviations. Here, the time-averaged probabilities are $\langle P_A(l) \rangle = \int_{t_0}^{t_e} P_A dt/(t_e - t_0)$ and $\langle P_B(l) \rangle = \int_{t_0}^{t_e} P_B dt/(t_e - t_0)$, where $t_0 = 100$, $t_e = 300$. The plot illustrates that the probabilities are independent of l at a large scale range $10 < l/\delta < 600$:

$$\langle P_A(l) \rangle = 0.575, \quad \langle P_B(l) \rangle = 0.425.$$

Namely, the probabilities satisfy scale invariance in the inertial range, which is the important feature of self-similarity and is the basis of the Markov process analysis below.

The Markov process, named after Russian mathematician Andrey Markov [31], is a time-varying random phenomenon for which a specific property (the Markov property) holds. The most famous Markov process is the Markov chain. In the real world, many processes belong to the Markov process, such as the Brownian motion of particles in a liquid, the animal

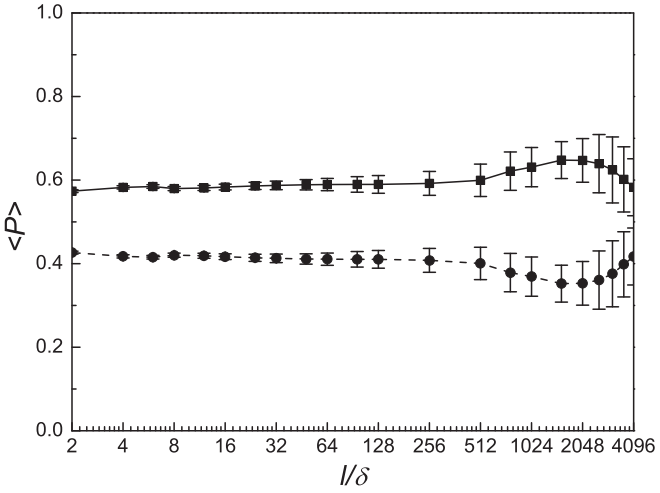

FIG. 7. Time-averaged probabilities for subensemble A (squares) and subensemble B (dots) at different scales. The corresponding error bars are also plotted.

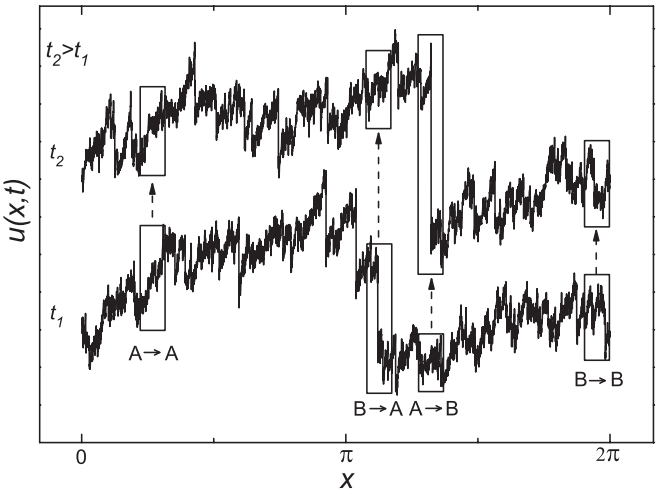

FIG. 8. Transitions between subensembles A and B from t_1 to t_2 with fixed structure scale in the Eulerian sense.

number change in a forest, the number of people infected by a disease, the number of people waiting for a bus in a station, the transition of free electrons in an atomic nucleus, population growth, some courses of inheritance, and so on. After Markov, many famous theorists in probability, statistics, mathematics, and physics have made important improvements on relative studies, such as Kolmogorov [32], Ito [33], Feller [34], Dynkin [35], Dvoretzky [36], and Hunt [37].

The Markov chain [38] is a sequence of stochastic variables, $X_1, X_2, X_3, \ldots$, with their range as a state space gathering all possible values, where X_n denotes the state at time t_n. A stochastic process has the Markov property if the conditional probability distribution of the future state X_{n+1} depends only upon the present state X_n; that is, given the present, the future does not depend on the past. This feature can be written with a probability form:

$$P(X_{n+1} = x|X_0, X_1, X_2, \ldots, X_n) = P(X_{n+1} = x|X_n).$$

During the Burgers equation evolution under the action of random forcing, the energy cascade at point x with fixed scale l changes between positive and negative directions. The transition appearing as the interconversion of shock and rarefaction waves is a kind of Markov process. Figure 8 shows a sketch about this feature in the Eulerian sense. There are totally four kinds of structure style transitions between A and B: $A \rightarrowtail A$, $A \rightarrowtail B$, $B \rightarrowtail A$, and $B \rightarrowtail B$. The key quantities to describe the Markov process are so-called transition probabilities, defined as

$$\begin{aligned} P_{AA}(l,t_1,\delta t) &= P(h(x,l,t_2) \geqslant 0 | h(x,l,t_1) \geqslant 0), \\ P_{AB}(l,t_1,\delta t) &= P(h(x,l,t_2) < 0 | h(x,l,t_1) \geqslant 0), \\ P_{BA}(l,t_1,\delta t) &= P(h(x,l,t_2) \geqslant 0 | h(x,l,t_1) < 0), \\ P_{BB}(l,t_1,\delta t) &= P(h(x,l,t_2) < 0 | h(x,l,t_1) < 0), \end{aligned} \tag{15}$$

where the time interval is $\delta t = t_2 - t_1$.

For $P_{AB} \equiv 1 - P_{AA}$ and $P_{BA} \equiv 1 - P_{BB}$, we need to only focus on two variables defined in Eqs. (15), such as P_{AA} and P_{BB}. Through statistical counting, we found that the transition probabilities are independent of the reference time point t_1 but depend only on the time interval δt at the stable state ($t_1 > 100$). The time averages of P_{AA} and P_{BB} at different scale l and time interval δt are defined as

$$\langle P_{AA}(l,\delta t)\rangle = \frac{1}{t_e - t_0}\int_{t_0}^{t_e} P_{AA}(l,t',\delta t)dt', \tag{16}$$

$$\langle P_{BB}(l,\delta t)\rangle = \frac{1}{t_e - t_0}\int_{t_0}^{t_e} P_{BB}(l,t',\delta t)dt', \tag{17}$$

where $t_0 = 100$ and $t_e = 300$. Figure 9 shows that when $\delta t = 163$ in the inertial range, like the probability of A and B, the four time-averaged transition probabilities are scale invariant, too. In fact, for a small time interval δt, the transition probability scale invariance is untenable.

Figures 10 and 11 display the changing of $\langle P_{AA}(l,\delta t)\rangle$ and $\langle P_{BB}(l,\delta t)\rangle$, respectively, with different time interval δt at different scales. Though the transition probability scale invariance is broken at a fixed small δt, we can see that all of the transition probabilities possess the similarity wherein

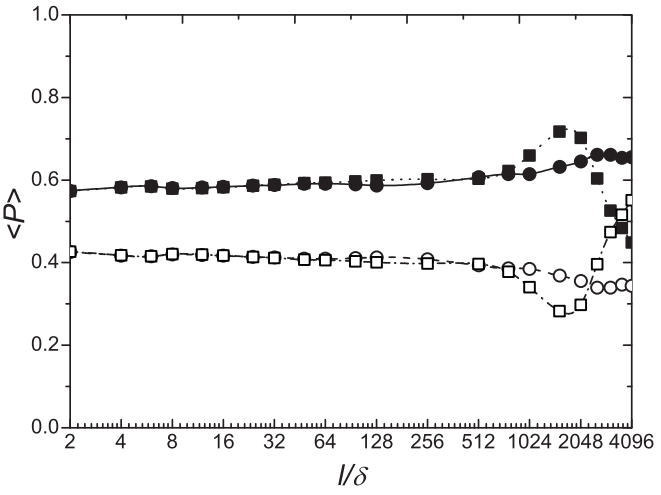

FIG. 9. Time average of the transition probabilities: $\langle P_{AA}(l,\delta t)\rangle$ (solid squares), $\langle P_{AB}(l,\delta t)\rangle$ (solid circles), $\langle P_{BB}(l,\delta t)\rangle$ (open squares), and $\langle P_{BA}(l,\delta t)\rangle$ (open circles).

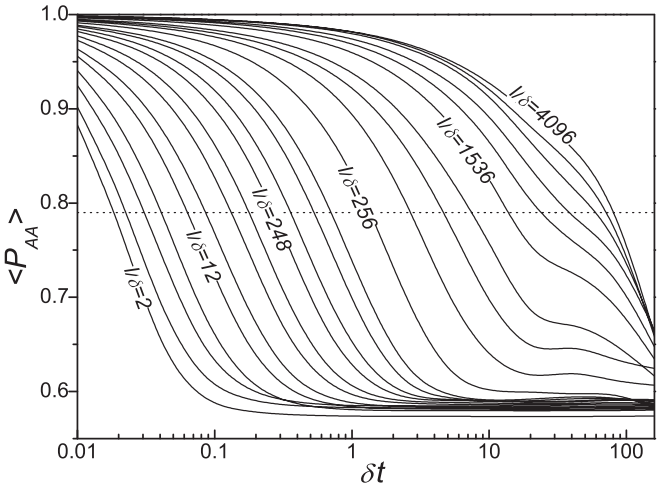

FIG. 10. Time average of the transition probabilities $\langle P_{AA}(l,\delta t)\rangle$. The dotted line corresponds to $\langle P_{AA}\rangle = (1+\langle P_A\rangle)/2$.

they gradually converge toward 1 when $\delta t \to 0$ and toward a constant when $\delta t \to +\infty$. As a simple explanation, the value $\langle P_{AA}(l,\delta t \to 0)\rangle \approx 1$ or $\langle P_{BB}(l,\delta t \to 0)\rangle \approx 1$ indicates the time is too short to change the structure style from one to the other.

To inspect the transition probability similarity, let us introduce the Chapman-Kolmogorov equation, which is often used to describe a Markov chain:

$$\begin{pmatrix} P_A(l,t_2) \\ P_B(l,t_2) \end{pmatrix} = \begin{pmatrix} P_{AA}(l,t_1,\delta t) & P_{BA}(l,t_1,\delta t) \\ P_{AB}(l,t_1,\delta t) & P_{BB}(l,t_1,\delta t) \end{pmatrix} \begin{pmatrix} P_A(l,t_1) \\ P_B(l,t_1) \end{pmatrix}. \tag{18}$$

Considering in the inertial range $10 < l/\delta < 600$,

$$\begin{aligned} P_A(l,t_1) &\approx P_A(l,t_2), \\ P_B(l,t_1) &\approx P_B(l,t_2), \\ P_{AB}(l,t_1,\delta t) &= 1 - P_{AA}(l,t_1,\delta t), \\ P_{BA}(l,t_1,\delta t) &= 1 - P_{BB}(l,t_1,\delta t), \end{aligned}$$

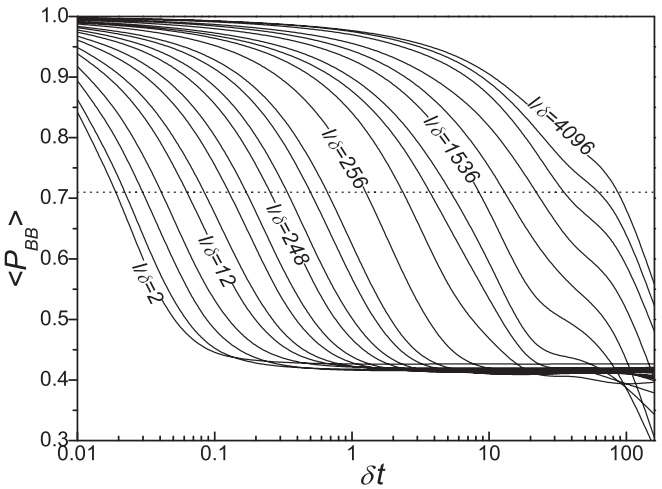

FIG. 11. Time average of transition probabilities $\langle P_{BB}(l,\delta t)\rangle$. The dotted line corresponds to $\langle P_{BB}\rangle = (1+\langle P_B\rangle)/2$.

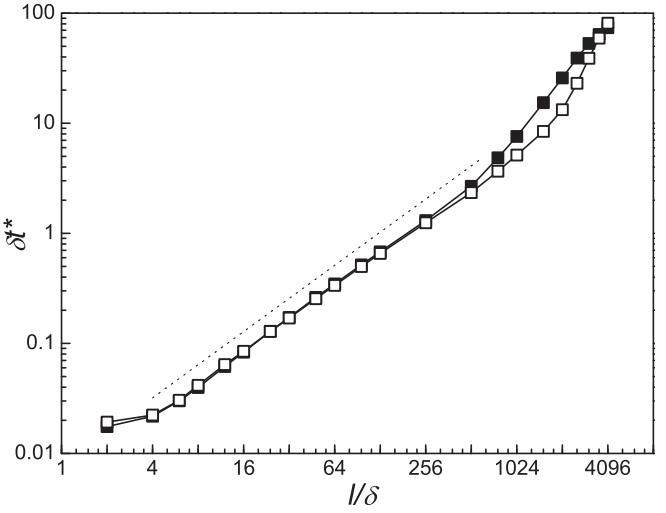

FIG. 12. Characteristic time of transition probabilities $\langle P_{AA}\rangle$ (solid squares) and $\langle P_{BB}\rangle$ (open squares) at different structure scale l. The dotted line has a slope of 1.

and, using the time-average form, we can derive a simple equation replacing Eq. (18):

$$\begin{pmatrix} \langle P_A(l)\rangle \\ \langle P_B(l)\rangle \end{pmatrix} = \begin{pmatrix} \langle P_{AA}(l,\delta t)\rangle & 1-\langle P_{BB}(l,\delta t)\rangle \\ 1-\langle P_{AA}(l,\delta t)\rangle & \langle P_{BB}(l,\delta t)\rangle \end{pmatrix} \begin{pmatrix} \langle P_A(l)\rangle \\ \langle P_B(l)\rangle \end{pmatrix}. \tag{19}$$

Figures 10 and 11 also tell us that when $\delta t \to +\infty$, $\langle P_{AA}(l,+\infty)\rangle \approx \langle P_A(l)\rangle$ and $\langle P_{BB}(l,+\infty)\rangle \approx \langle P_B(l)\rangle$, which is just right—a group solution of Eq. (19). Similarly, $\langle P_{AA}(l,0)\rangle \approx 1$ and $\langle P_{BB}(l,0)\rangle \approx 1$ make up another group solution of Eq. (19). Meanwhile, the speeds of the transition matrices going to the above two special solutions are different at different structure scales.

Here, we define a so-called characteristic time $\delta t^*(l)$ to normalize $\langle P_{AA}(l,\delta t)\rangle$ and $\langle P_{BB}(l,\delta t)\rangle$, respectively. For example, the characteristic time $\delta t^*(l)$ is equal to the horizontal ordinate value of crossing points between the line $\langle P_{AA}\rangle = (1+\langle P_A\rangle)/2$ and the lines $\langle P_{AA}(l,\delta t)\rangle$ in Fig. 10. The measured characteristic times at different l/δ are shown in Fig. 12 and markedly satisfy line functions with slope close to 1 in the inertial range,

$$\delta t^*(l) = C_t(l/\delta)^\alpha, \quad 10 < l/\delta < 600, \tag{20}$$

where $\alpha \approx 1$ and C_t is a system parameter.

Using the data in Fig. 12, we redraw Figs. 10 and 11 as Fig. 13, where the horizontal ordinates are replaced by $\delta t/\delta t^*$. Clearly, all the transition probabilities, $\langle P_{AA}\rangle$ and $\langle P_{BB}\rangle$, collapse together as two curves with specific lower bounds, which satisfy the function

$$\langle P_{\beta\beta}(l,\delta t)\rangle = [1-\langle P_\beta(l)\rangle]\left(\tfrac{1}{2}\right)^{\delta t/\delta t^*(l)} + \langle P_\beta(l)\rangle, \tag{21}$$

where β represents A or B. In the plot, some points departing from the curves are those out of the inertial range.

So based on the stationary transition probability matrix, $\langle P_{\beta\beta}(l,\delta t)\rangle \approx P_{\beta\beta}(l,\delta t)$, a collapsed Markov chain [39] has

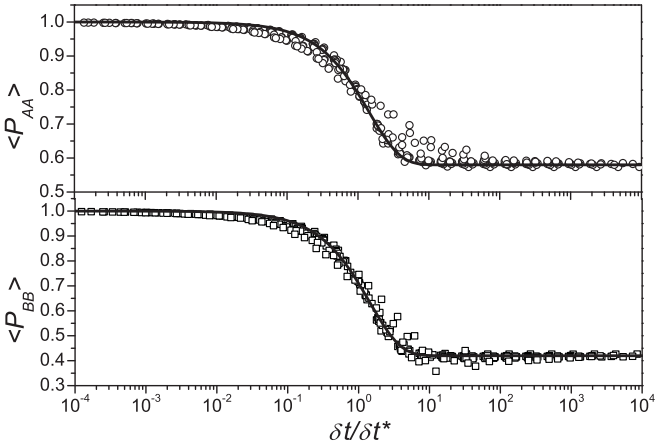

FIG. 13. Transition probabilities $\langle P_{AA}(l,\delta t/\delta t^*)\rangle$ (top) and $\langle P_{BB}(l,\delta t/\delta t^*)\rangle$ (bottom). The solid lines correspond to Eq. (21).

been built in fact. The probability $\langle P_\beta\rangle$ in Eq. (21) is found to depend mainly on the random force $f(x,t)$, especially the spectral exponent y in Eq. (5).

V. EFFECTS OF RANDOM FORCING PARAMETER y

In order to probe the effects of random forcing on the Burgulence field, we carried out five DNS cases with parameters $y = 0.25$, 0.5, 0.75, 1.0, and 2.0 in Eq. (5), respectively, and the other computation conditions were set identically as in the case $y = 1.0$ discussed above. Using the subensemble decomposition method explained in Sec. III, we obtained some statistical results for each case, shown in Table I.

Figure 14 shows the energy spectra of the five Burgulence fields. In the plot, the slopes of the log-log plot of energy spectra in the inertial range are monotone decreasing functions of y, which deviates from Yakhot's prediction, $E(k) \propto k^{-5/3+2/3(d-y)}$, deduced in Ref. [40], where the dimension $d = 1$. When y is large, e.g., $y = 2.0$, the velocity field is close to a decaying Burgulence field with energy spectrum slope -2, which means the random forcing effect can be ignored. On the other hand, when y becomes smaller, the random forcing is bigger, the velocity field seems more like white noise, and the energy spectrum is flatter. Furthermore, a demonstrable proposition is that, when the energy spectrum becomes flatter and flatter, the entire average local energy flux at the same scale refers less and less to the total kinetic energy, which indicates that the relative difference between the average positive and negative local energy fluxes is smaller. So when y is small enough, the phenomenon of the whole field being dominated by shock is no longer apparent.

TABLE I. DNS cases and statistical quantities for Burgulence with different parameter y.

Case	y	$E(k)$	Slope of $\zeta_{p,A}$	$\langle P_A\rangle$
1	0.25	$\propto k^{-1.209}$	0.137	0.523
2	0.50	$\propto k^{-1.402}$	0.200	0.537
3	0.75	$\propto k^{-1.545}$	0.273	0.556
4	1.00	$\propto k^{-1.657}$	0.334	0.575
5	2.00	$\propto k^{-2.005}$	0.630	0.664

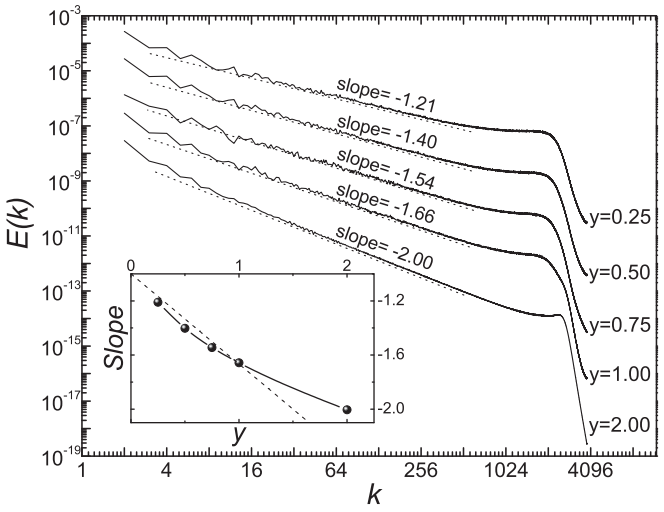

FIG. 14. Energy spectrum averaged in $t \in [100,300]$ (solid line) with $y = 0.25$, 0.5, 0.75, 1.0, and 2.0, respectively. The slopes are plotted in the inset, in which the dotted line show Yakhot's prediction.

Another important and interesting result is that all of the exponents for subensemble A exhibit linear scaling behaviors, and the slopes of $\zeta_{p,A}$ vs p form a monotone increasing function of y within inertial range,

$$\zeta_{p,A} \approx \frac{yp}{3},$$

which is shown in the inset of Fig. 15. At the same time, we can see from Fig. 15 that the scaling behaviors of subensemble B in all of the five cases are anomalous. The exponents of subensemble B converge toward a different constant with different y at high orders p. Thus the shock waves, the positive energy fluxes, dominate the intermittency of Burgulence, but the domination level is lower when y is small, in which case the scaling behaviors of subensembles A and B are close together. By the way, the total kinetic energy is at a high level with the same other conditions, though the relative energy fluxes

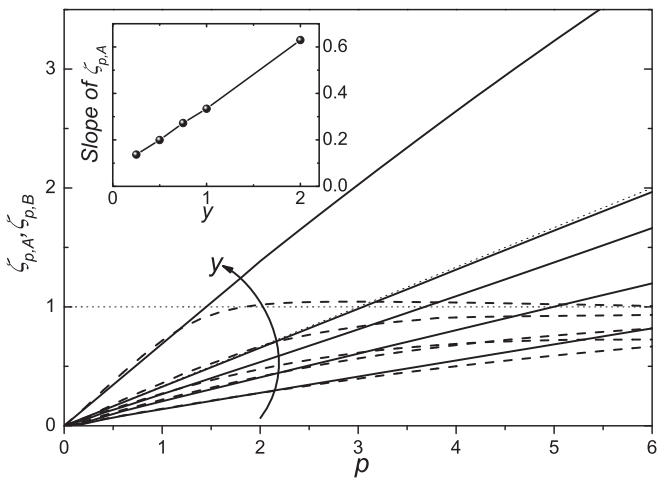

FIG. 15. Exponents of structure function for subensemble A (solid lines) and subensemble B (dashed lines) with y increasing in the direction of the arrow. The horizontal dotted line and the inclined oblique dotted line correspond to constant 1 and $p/3$, respectively. The inset shows the slopes of $\zeta_{p,A}$ vs y.

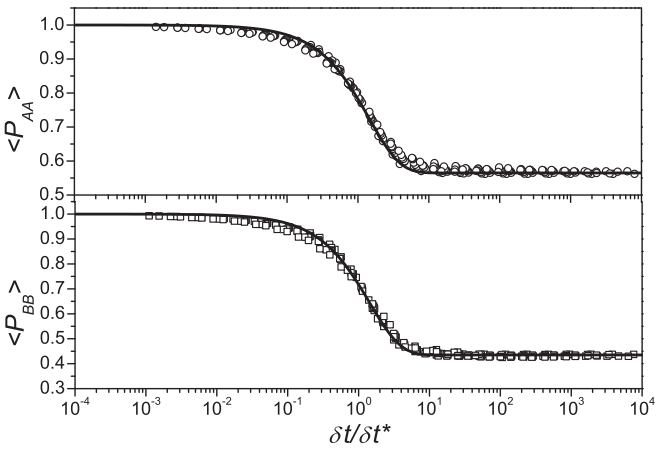

FIG. 16. Transition probabilities $\langle P_{AA}(l,\delta t/\delta t^*)\rangle$ (top) and $\langle P_{BB}(l,\delta t/\delta t^*)\rangle$ (bottom) with $y = 0.75$. The solid lines correspond to Eq. (21).

are small at small y, when the field receives its statistical equilibrium.

At last, following the Markov analysis in Sec. IV, we obtained the collapsed time-averaged transition probabilities $\langle P_{AA}(l,\delta t/\delta t^*)\rangle$ and $\langle P_{BB}(l,\delta t/\delta t^*)\rangle$ shown in Fig. 16 for the case $y = 0.75$. In this case, the relationship of Eq. (21) still holds with new different parameters, which mainly correspond to the characteristic times and the subensemble probabilities. Considering the comparison among the five cases, we can conclude that the smaller y is, the more the random forcing dominates the Burgulence field; and the smaller the probability of subensemble A is, the smaller the characteristic time is involved in changing from one state to another.

VI. CONCLUSION AND DISCUSSION

This paper presents a description of the transition between the positive and negative local energy fluxes, or the shock and rarefaction waves, from the angle of subensemble decomposition. Using the concept of GVD, we divide the Burgulence field into subensembles A and B, corresponding to rarefaction waves and shock waves. These two subensembles possess probability scale invariance in the inertial range and show the K41 scaling law and typical Burgers anomalous scaling law, respectively, which correspond to two different energy flux or cascade processes. Furthermore, we investigate the interconversion between A and B through Markov process analysis and find the elements of the transition probability matrix in the stationary Chapman-Kolmogorov equation, Eq. (19), fit a universal form at different scales, namely Eq. (21), which offers an uncomplicated probabilistic description for the structure evolution and exhibits some additional properties of nonlinear dynamic self-organization in Burgulence.

Since similarities exist between 1D Burgulence and 3D Navier-Stocks turbulence, the statistical analysis method proposed here can be applied to 3D turbulence, too. In the 3D case, the local energy flux can be defined as [29]

$$\Pi(\mathbf{x},l) = -\frac{\partial\langle u_i\rangle_l}{\partial x_j}\tau_{ij} = -\frac{\partial\langle u_i\rangle_l}{\partial x_j}(\langle u_i u_j\rangle_l - \langle u_i\rangle_l\langle u_j\rangle_l),$$

where $\langle\cdot\rangle_l$ denotes the average at scale l. If the integral energy flux is nonzero, the distribution of local energy fluxes is asymmetric about zero, and the scaling behaviors may be different in the two subensembles, corresponding to positive and negative signs of $\Pi(\mathbf{x},l)$, respectively.

Another important issue is introducing the Lagrangian description to study the Markov process of subensemble transition process, which displays a similar and more physical visualized pattern, we think. In addition, the two kinds of different cascade properties indicate that a large eddy simulation may be erected based on the subensemble decomposition idea. Beyond statistical theory, the concept itself of ensemble or subensemble decomposition in the sense of self-organization [41] offers a simple hydrodynamic training ground for developing mathematical tools to study not only turbulence but also multistructure, multiscale, multistate, or Lagrangian problems.

ACKNOWLEDGMENTS

This work is supported by the National Science Foundation of China (Grant No. 90716008) and the MOST of China (973 Project No. 2009CB724100). The authors wish to thank Y. Shi, M. Zhou, J. Chen, H. Guo, K. Ding, and Y. Wang for helpful discussions.

[1] A. Kolmogorov, Dokl. Akad. Nauk SSSR **32**, 16 (1941) [Proc. R. Soc. London, Ser. A **343**, 15 (1991)].
[2] R. H. Kraichnan, Phys. Fluids **10**, 2080 (1967).
[3] R. H. Kraichnan, J. Fluid Mech. **62**, 305 (1974).
[4] U. Frisch and J. Bec, in *Les Houches 2000*, edited by M. Lesieur (Springer, Berlin, 2001), p. 341.
[5] J. Bec and K. Khanin, Phys. Rep. **447**, 1 (2007).
[6] J. M. Burgers, Trans. Roy. Neth. Acad. Sci. Amsterdam, Phys.-Sci. **17**, 1 (1939).
[7] E. Hopf, Commun. Pure Appl. Math. **3**, 201 (1950).
[8] J. D. Cole, Quart. Appl. Math. **9**, 225 (1951).
[9] W. C. Meecham and A. Siegel, Phys. Fluids **7**, 1178 (1964).
[10] I. Hosokawa and K. Yamamoto, Phys. Fluids **13**, 1683 (1970).
[11] D. T. Jeng, Phys. Fluids **12**, 2006 (1969).
[12] M. Avellaneda and E. Weinan, Commun. Math. Phys. **172**, 13 (1995); M. Avellaneda, *ibid.* **169**, 45 (1995).
[13] D. Forster, D. R. Nelson, and M. J. Stephen, Phys. Rev. Lett. **36**, 876 (1976); Phys. Rev. A **16**, 732 (1977).
[14] A. Chekhlov and V. Yakhot, Phys. Rev. E **51**, R2739 (1995); **52**, 5681 (1995).
[15] A. Kolmogorov, Dokl. Akad. Nauk SSSR **30**, 9 (1941) [Proc. R. Soc. London, Ser. A **343**, 9 (1991)].
[16] A. Kolmogorov, C. R. (Dokl.) Acad. Sci. URSS **31**, 538 (1941).
[17] A. M. Polyakov, Phys. Rev. E **52**, 6183 (1995).
[18] J. P. Bouchaud, M. Mézard, and G. Parisi, Phys. Rev. E **52**, 3656 (1995).
[19] V. Yakhot and A. Chekhlov, Phys. Rev. Lett. **77**, 3118 (1996).

[20] O. Zikanov, A. Thess, and R. Grauer, Phys. Fluids **9**, 1362 (1997).
[21] V. Yakhot, Phys. Rev. E **57**, 1737 (1998).
[22] E. Weinan and E. Vanden Eijnden, Phys. Rev. Lett. **83**, 2572 (1999).
[23] A. I. Chernykh and M. G. Stepanov, Phys. Rev. E **64**, 026306 (2001).
[24] J. Bec, U. Frish, and K. Khanin, J. Fluid Mech. **416**, 239 (2000).
[25] J. Bec, Phys. Rev. Lett. **87**, 104501 (2001).
[26] S. Boldyrev, T. Linde, and A. Polyakov, Phys. Rev. Lett. **93**, 184503 (2004).
[27] D. Mitra, J. Bec, R. Pandit, and U. Frisch, Phys. Rev. Lett. **94**, 194501 (2005).
[28] J. M. Burgers, *The Nonlinear Diffusion Equation* (Reidel, Boston, 1974).
[29] G. L. Eyink, J. Stat. Phys. **78**, 335 (1995).
[30] Z. S. She and E. Leveque, Phys. Rev. Lett. **72**, 336 (1994).
[31] A. A. Markov, Bull. Soc. Phys. Math. **15**, 135 (1906).
[32] A. N. Kolmogorov, Math. Ann. **104**, 415 (1931); **112**, 155 (1936).
[33] K. Itô, Mem. Amer. Math. Soc. **4**, 1 (1951).
[34] W. Feller, Trans. Am. Math. Soc. **77**, 1 (1954); Ann. Math. **60**, 417 (1954).
[35] E. B. Dynkin, Theory Probab. Appl. **1**, 22 (1956); **1**, 34 (1956).
[36] A. Dvoretzky, P. Erdös, and S. Kakutani, Acta Sci. Math. Szeged **12**, 75 (1950); *Proceedings of the Fourth Berkeley Symposium on Mathematical Statistics and Probability* (University of California Press, Berkeley, CA, 1961), Vol. 2, p. 103.
[37] G. A. Hunt, Illinois J. Math. **1**, 44 (1957).
[38] A. A. Markov, in *Dynamic Probabilistic Systems, Volume 1: Markov Chains*, edited by R. Howard (Wiley, New York, 1971), App. B.
[39] J. Hachigian, Ann. Math. Stat. **34**, 233 (1963).
[40] V. Yakhot and S. A. Orszag, J. Sci. Comput. **1**, 3 (1986).
[41] Z. S. She and Z. X. Zhang, Acta Mech. Sin. **25**, 279 (2009).